*Kovove Mater. 61 2023 277–283*
*DOI: 10.31577/km.2023.5.277*


# Formation mechanism of surface exudation in CuSn alloy prepared by horizontal continuous unidirectional solidification

Jihui Luo[1]*, Ting Liu[2], Suting Wei[2], Fang Qin[2], Yongda Mo[3]

[1] *College of Materials Science and Engineering, Yangtze Normal University, Chongqing, P. R. China*
[2] *School of Civil and Architectural Engineering, Yangtze Normal University, Chongqing, P. R. China*
[3] *School of Materials Science and Engineering, University of Science and Technology Beijing, Beijing, P. R. China*

Received 15 December 2022, received in revised form 20 March 2023, accepted 25 April 2023

**Abstract**

The Cu-5wt.%Sn alloy was prepared by using the horizontal continuous unidirectional solidification (HCUS) technique. The microstructure of HCUS Cu-5wt.%Sn alloy was analyzed by optical microscope and scanning electron microscope. Meanwhile, numerical simulation software ProCAST was used to simulate the Sn distribution of HCUS Cu 5wt.%Sn alloy. The results show that there exists a serious exudation layer on the lower surface of the HCUS Cu-5wt.%Sn alloy, while there is almost no exudation layer on the upper surface of the alloy. The simulation results show that the solid-liquid interface in the center protrudes to the liquid during the HCUS process. A narrow gap is formed between the mold and the alloy. During solidification, Sn solute is precipitated from solid to liquid. Therefore, the liquid between dendrites has a low melting point and does not solidify at high mold temperatures. These liquids flow down into the gap due to gravity and solidify at the last stage, forming an exudation layer on the lower surface enriched by Sn solute.

K e y w o r d s: continuous unidirectional solidification, CuSn alloy, exudation, numerical simulation

## 1. Introduction

The alloy with columnar crystal, prepared by continuous unidirectional solidification (CUS) [1, 2], has high conductivity [4] and plasticity [5] due to the fact that there are few or no grain boundaries. However, there exists an exudation layer on the surface of the CUS alloy [6, 7], which seriously affects the secondary processing performance of the alloy. It is generally believed that the formation of the exudation layer is the result of inverse segregation [8–10]. Another theory is that the alloy solidification starts from the surface and condenses into a shell. The metal liquid rich in solute moves to the surface under the action of external force and reaches the surface of the alloy through the gap between the solidified shells, thus forming the phenomenon of surface segregation. The main functions of external force include solidification shrinkage force, gravity, pressure of the indenter, etc. [11, 12]. However, the above mechanism cannot explain the phenomenon of surface segregation or exudation layer in CUS alloys. Luo [13] studied the reason for the formation of the surface exudation layer of the vertical CUS AlCu alloy. The results showed that it was related to the solid-liquid interface morphology. In the vertical CUS process, a narrow gap was formed between the mold and the alloy edge. The gap was filled with solute-rich liquid metals that started solidifying in the final stages of solidification, forming an exudation layer.

In order to further explain and analyze the formation mechanism of the exudation layer in CUS alloy, the horizontal CUS (HCUS) technique was used to prepare Cu-5wt.%Sn alloy with a diameter of 10 mm. The distribution of Sn solute in HCUS Cu-5wt.%Sn alloy was analyzed. The formation mechanism of the exudation layer of HCUS Cu-5wt.%Sn alloy was discussed.

*Corresponding author: e-mail address: 20170128@yznu.cn

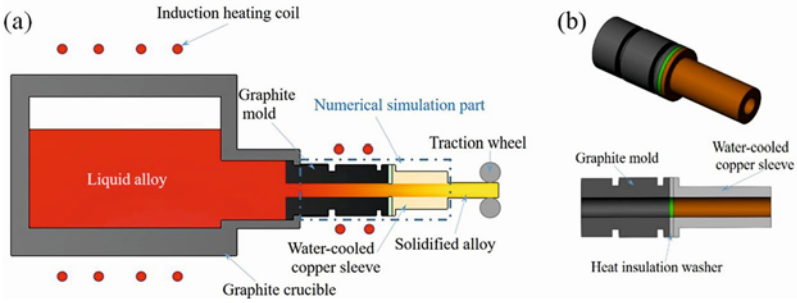


Fig. 1. Schematic diagram of HCUS: (a) HCUS device and (b) mold and cooling device.

## 2. Experimental

### 2.1. HCUS CuSn alloy experiment

In this experiment, Cu-5wt.%Sn alloy was selected as the raw material. According to Cu-Sn alloy phase diagram, it can be found that the liquidus temperature of the alloy is 1050 ℃. Figure 1a shows the schematic diagram of HCUS equipment. The Cu-5wt.%Sn alloy was melted in the graphite crucible by using an induction heating coil. Then, the melting alloy will flow into the graphite mold. Meanwhile, the graphite mold was also heated by an induction heating coil. Therefore, the mold temperature can be controlled above the liquidus temperature of the alloy. At the mold exit, a water-cooled copper sleeve was set to force-cool the solidified alloy. The traction wheels were installed to continuously pull out the solidified alloy from the graphite mold. Figure 1b shows the detailed structures of the graphite mold and water-cooled copper sleeve.

The Cu5wt.%Sn alloy in the graphite crucible was melted at 1150 ℃, and the mold temperature was controlled at 1080 ℃. A pure copper dummy bar with a diameter of 10 mm was inserted into the mold. With the liquid Cu-5wt.%Sn alloy in the crucible continuously feeding into the mold, the alloy would be welded with the dummy bar. Then, the Cu-5wt.%Sn alloy was forced to cool by the water-cooled copper sleeve at the mold exit. The temperature of the cooling water was 20 ℃. Hereafter, the Cu-5wt.%Sn alloy with a diameter of 10 mm was continuously pulled out at a speed of 10 mm min$^{-1}$ by traction wheels.

### 2.2. Numerical simulation of HCUS Cu-5wt.%Sn alloy

Numerical simulation was performed by ProCAST software for the mold and alloy in the dash-dotted line frame in Fig. 1a. Because the mold and alloy were axially symmetric, the two-dimensional model was established. The mold was divided into triangular mesh with an edge length of 1.5 mm. According to different positions, the models of an upper surface and lower surface were established, as shown in Figs. 2a,b.

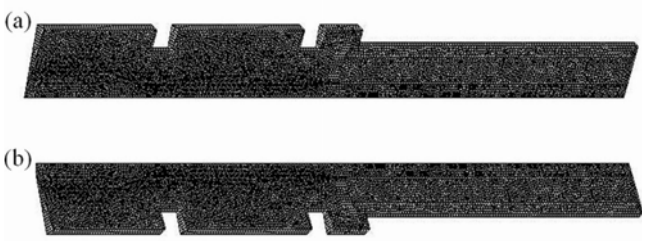


Fig. 2. Two-dimensional model of mold and alloy: (a) upper surface and (b) lower surface.

The gravity direction was downward. The processing parameters of the simulation were as follows: the melting temperature of 1150 ℃, the mold temperature of 1080 ℃, continuous casting speed of 10 mm min$^{-1}$, and cooling water temperature of 25 ℃.

Governing equations (Eqs. (1)–(4)) are as follows [14, 15]:

– the continuity equation:

$$\frac{\partial \rho}{\partial t} + \frac{\partial \rho_{\mathrm{u}}}{\partial x} + \frac{\partial \rho_{\mathrm{v}}}{\partial y} + \frac{\partial \rho_{\mathrm{w}}}{\partial z} = 0, \tag{1}$$

– the momentum equation:

$$\frac{\rho}{f_{\mathrm{L}}}\frac{\partial v}{\partial t} + \frac{\rho}{f_{\mathrm{L}}^2}\left(\mu\frac{\partial v}{\partial x} + v\frac{\partial v}{\partial y} + w\frac{\partial v}{\partial z}\right) = -\frac{\partial P}{\partial y} + \rho g_{\mathrm{x}} + \frac{\partial}{\partial x}\left(\frac{v}{f_{\mathrm{L}}}\frac{\partial v}{\partial x}\right) + \frac{\partial}{\partial y}\left(\frac{v}{f_{\mathrm{L}}}\frac{\partial v}{\partial y}\right) + \frac{\partial}{\partial z}\left(\frac{v}{f_{\mathrm{L}}}\frac{\partial v}{\partial z}\right) - \left(\frac{\mu}{K}\right)v, \tag{2}$$

– the energy equation:

$$\rho\frac{\partial H}{\partial t} + \rho\frac{\partial H}{\partial T}\left(\mu\frac{\partial T}{\partial x} + v\frac{\partial T}{\partial y} + w\frac{\partial T}{\partial z}\right) = \frac{\partial}{\partial x}\left(k\frac{\partial T}{\partial x}\right) + \frac{\partial}{\partial y}\left(K\frac{\partial T}{\partial y}\right) + \frac{\partial}{\partial z}\left(k\frac{\partial T}{\partial z}\right), \tag{3}$$

where $H(T)$ is given by

$$H(T) = \int_0^T C_{\mathrm{P}}\mathrm{d}t + L\left[1 - f_{\mathrm{S}}(T)\right], \tag{4}$$

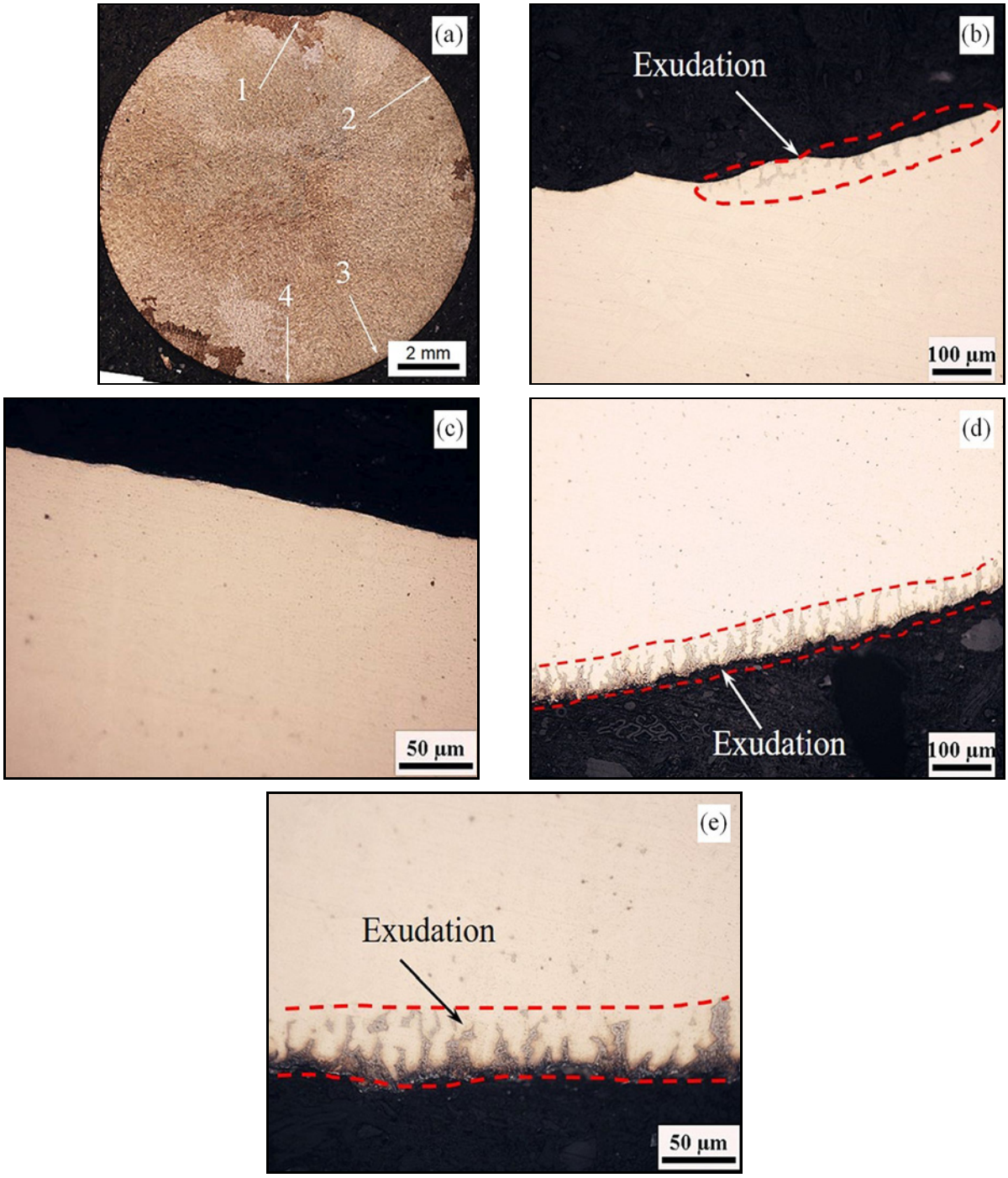


Fig. 3. Cross-section of microstructure of HCUS Cu-5wt.%Sn alloy: (a) cross-section of over-all microstructure, (b) upper surface, (c) upper side surface, (d) lower side surface, and (e) lower surface.

where $u$, $v$, and $w$ are the velocity components of the $x$, $y$, and $z$ directions, respectively, ($\mathrm{m\,s^{-1}}$); $f_\mathrm{L}$ is the liquid fraction (vol.%); $f_\mathrm{s}$ is the solid fraction, (vol.%); $P$ is the pressure, (Pa); $g_\mathrm{x}$ is the gravity component of the $x$ direction, ($\mathrm{m\,s^{-2}}$); $\rho$ is the density of steel, ($\mathrm{kg\,m^{-3}}$); $\mu$ is the absolute viscosity, (Pa s); $k$ is the thermal conductivity, ($\mathrm{W\,m^{-1}\,K^{-1}}$); $K$ is the permeability, ($\mathrm{m^2}$); $C_\mathrm{P}$ is the specific heat capacity of alloy, ($\mathrm{J\,kg^{-1}\,K^{-1}}$); $t$ is the time, (s); $L$ is the latent heat of solidification, ($\mathrm{J\,kg^{-1}}$); $T$ is the junction temperature, (K); $H$ is the enthalpy, ($\mathrm{J\,mol^{-1}}$); and $x$, $y$, and $z$ are the rectangular coordinates.

In order to simplify the simulation, the HCUS process was assumed as follows:

(1) Based on the steady-state simulation, only the temperature fields, reaching a steady state under the boundary condition, were considered;

(2) Physical parameters and heat transfer coeffi-

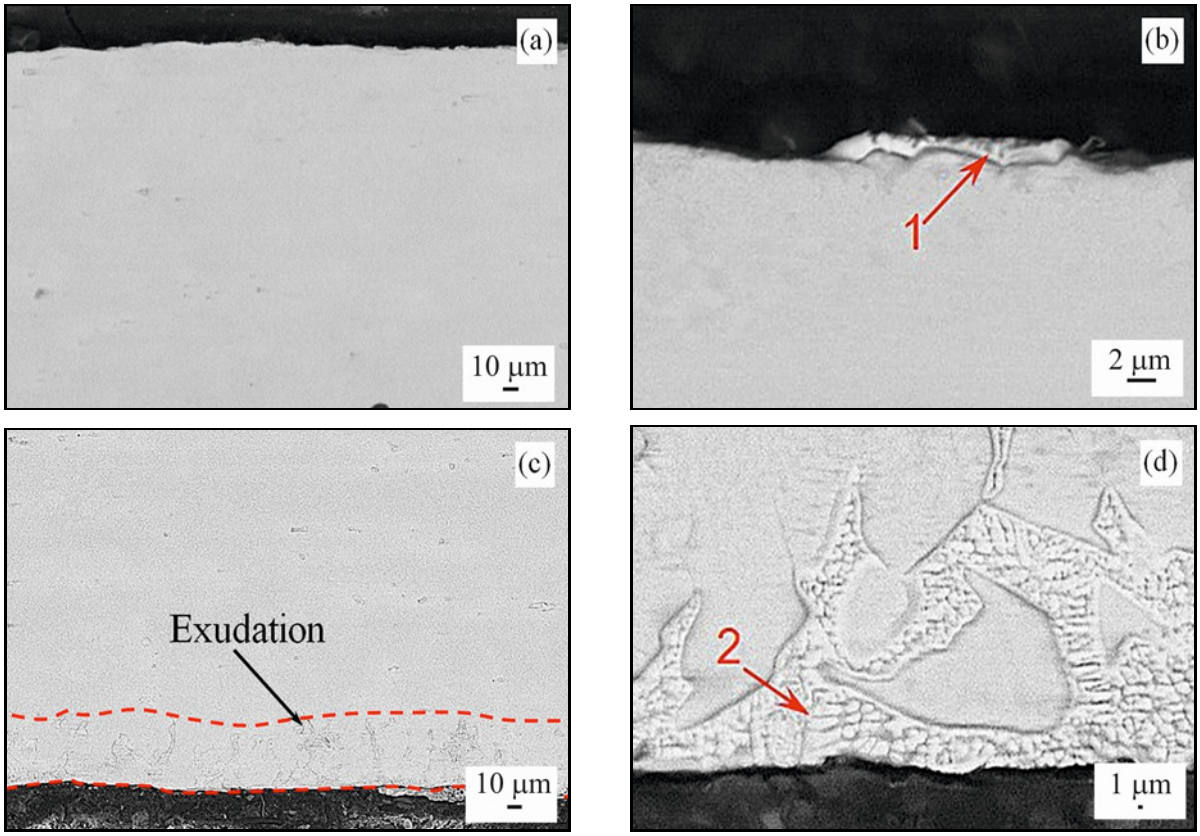


Fig. 4. SEM morphology of HCUS Cu-5wt.%Sn alloy: (a) and (b) upper surface of the alloy; (c) and (d) lower surface of the alloy.

cient were only related to temperature;

(3) The cooling water was evenly distributed in the circumferential direction, and the cooling intensity was identical.

### *2.3. Microstructure observation*

The samples were taken from the HCUS Cu--5wt.%Sn alloy and etched by corrosion solution of ferric chloride (5 g) and anhydrous ethanol (100 mL). The microstructure was observed by optical microscope and field emission scanning electron microscope (SEM). Energy dispersive spectrometry (EDS) was used to analyze the chemical composition.

## 3. Results and discussion

### *3.1. Microstructure of HCUS Cu-5wt.%Sn alloy*

Figure 3a shows the cross-section microstructure of HCUS Cu-5wt.%Sn alloy. In Fig. 3a, arrows 1 and 4 represent the position of the upper surface and the lower surface of the HCUS Cu-5wt.%Sn alloy. The remaining arrows 2 and 3 represent the upper side surface and lower side surface. Figure 3b is a further enlargement of the upper surface, which is indicated by arrow 1 in Fig. 3a. There exists a small amount of exudation. Figure 3c is a further enlargement of the upper side surface, which is indicated by arrow 2 in Fig. 3a. It can be found that there does not exist exudation, and the microstructure at the alloy edge is relatively uniform. Figures 3d,e are further enlargements of the lower side surface and lower surface. A more serious exudation with a thickness of about 50 μm began to appear on the surface of the HCUS Cu-5wt.%Sn alloy.

Figure 4a shows the SEM morphology near the upper surface. It can be seen from Fig. 4a that there is no obvious exudation layer on the upper surface. Figure 4b is a further enlargement of Fig. 4a. A small amount of exudation is found, and the exudation thickness is about 1 μm. EDS analysis of point 1 in Fig. 4b shows that Sn content is 8.02 wt.%, which is higher than that of nominal alloy composition. Figure 4c shows the SEM morphology near the lower surface. There exists an exudation layer on the lower surface. Figure 4d is a further magnification of Fig. 4c. The exudation thickness reaches 20 μm. EDS analysis of point 2 in Fig. 4d shows that Sn content is 11.12 wt.%, which is much higher than that of the nominal composition of the alloy. The above experimental results indicate that HCUS Cu-5wt.%Sn alloy has surface segregation

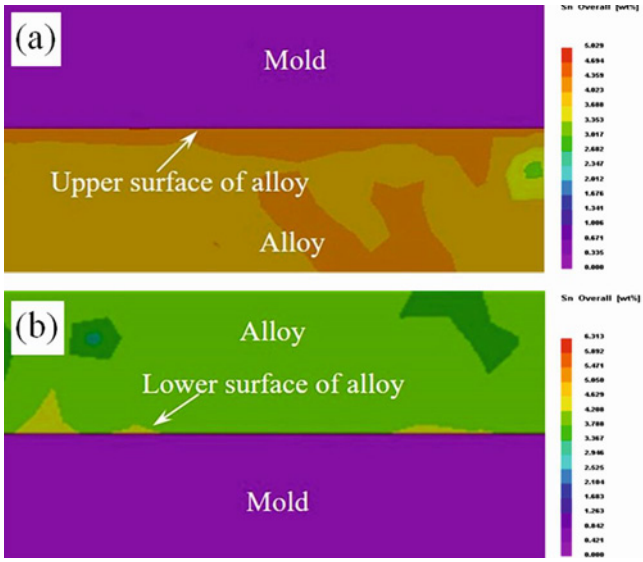


Fig. 5. Simulation results of Sn solute distribution: (a) upper surface and (b) lower surface.

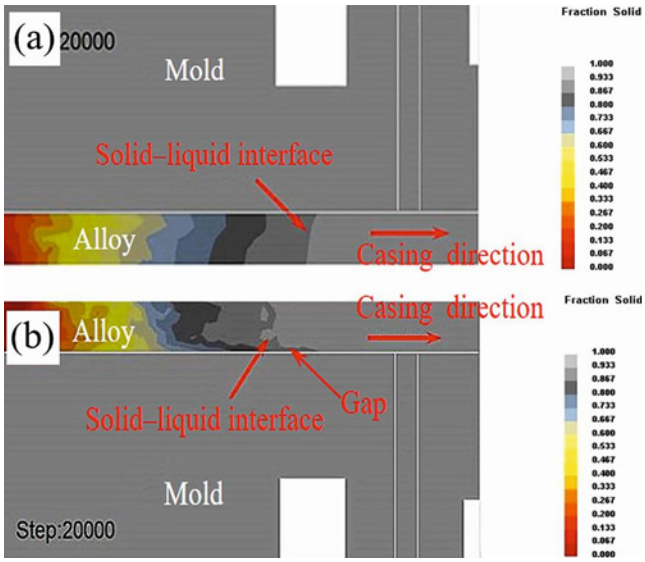


Fig. 6. Simulation results of solid-liquid interface morphology of HCUS Cu-5wt.%Sn alloy: (a) upper surface and (b) lower surface.

of Sn at the lower surface, forming a serious exudation layer.

### 3.2. Simulation results of HCUS Cu-5wt.%Sn alloy

Figure 5 is the simulation result of the Sn solute distribution of the HCUS Cu-5wt.%Sn alloy. Figure 5a shows the distribution of Sn solute on the upper surface of the alloy. Different colors represent the different Sn contents as shown on the right side of Fig. 5a. The Sn content in the center of the alloy is between 3.4 and 4.0 wt.%, and in the upper surface is between 4.0 and 4.3 wt.%. Figure 5b shows the distribution of Sn solute on the lower surface of the alloy. The Sn content in the center of the alloy is between 3.4 and 4.2 wt.%, and on the lower surface is between 4.6 and 5.0 wt.%.

From the above simulation results, it can be found that the alloy prepared by HCUS technology has a different Sn content in different parts. The Sn content is higher on the surface and is lower in the center of the alloy. At the lower surface, the Sn content reaches the highest value. The above simulation results agree with that of Sn content in experiments.

The solid-liquid interface of the HCUS Cu-5wt.%-Sn alloy process was simulated. Figure 6 shows the simulation results. Figure 6a shows the morphology of the solid-liquid interface on the upper surface. The gray color represents solid, and the red color represents liquid. The transition from gray to red color represents the solid fraction, and specific values can refer to the right side of the figure legend. The solid-liquid interface in the center of the alloy protrudes into the liquid. The solid-liquid interface at the edge of the alloy has a concave shape. This is attributed to the reason that the cooling-water force cools the solidified alloy at the mold exit. Therefore, the center of the alloy begins to solidify first.

Figure 6b shows the solid-liquid interface morphology of the lower surface. The solid-liquid interface in the center of the alloy also protrudes toward the liquid. Therefore, a narrow gap is formed between the alloy and the mold. From Figs. 5, 6, it can be found that when a narrow gap is formed, it always starts to appear with the exudation layer. On the contrary, there will be no exudation layer. Therefore, the formation of a narrow gap is an important reason affecting the formation of the exudation layer.

### 3.3. Discussion

During the solidification process, solute redistribution occurs. Sn solute is precipitated from the solid to the liquid, thus, leading to the decrease of solute content in the solid and the increase of solute content in the liquid. Since the solidification of the alloy starts from the center of the alloy, the Sn content in the center of the alloy starts to decrease as the solid ratio gradually increases, as shown in Fig. 5.

Because the alloy in contact with the mold is affected by the mold temperature, which is controlled above the solidus temperature of the alloy, the solid-liquid interface of the alloy near the edge has a slow growth rate to the mold wall, resulting in a gap formed between the mold and the alloy, as shown in Fig. 6. Sn solute can be precipitated during the transition from liquid to solid. While the solid-liquid interface at the alloy surface slowly proceeds towards one side of the

mold, a large amount of precipitated Sn solute will be assembled in inter-dendrites or the gap. Because liquid with enriched Sn solution has a low melting point, this liquid at the gap does not rapidly solidify in the high-temperature mold. Due to gravity, the liquid with a low melting point on the upper surface of the alloy begins to move downward. Thus, there exists a fewer Sn segregation on the upper surface of the HCUS Cu--5wt.%Sn alloy.

On the lower surface of the alloy, there also exists liquid that enriched Sn solute with a low melting point in the gap. Unlike the upper surface, the Sn solute precipitated from the solid will enter the narrow gap. These low-melting liquids cannot be solidified in the high-temperature mold, which in turn affects the movement of the solid-liquid interface toward the gap. Therefore, the length of the narrow gap is further increased (as shown in Fig. 6b). The liquids-enriched Sn solute becomes the surface layer and solidifies at last, thus leading to the formation of a macroscopic Sn segregation layer on the surface of the HCUS Cu--5wt.%Sn-alloy.

On the other hand, with the HCUS process, Cu--5wt.%Sn alloy is drawn out of the mold gradually, so the temperature near the mold exit is low. The nucleation on the wall occurs in the gap. While the equiaxed grains begin to nucleate and grow, Sn solute redistribution occurs between the equiaxed grains and the liquid in the gap. These equiaxed grains and precipitated Sn solute are enclosed in the root of the grains, which also can increase the amount of Sn content on the alloy surface.

Figure 7 shows the microstructure of HCUS Cu--5wt.%Sn alloy, and Fig. 7a is the microstructure of the HCUS Cu-5wt.%Sn alloy on the upper surface. The equiaxed grains appear on the upper surface. These equiaxed grains nucleate at the mold wall and do not completely fall off the mold wall, or the distance from the mold wall is short. It is too late to move to the center of the alloy, and they are enclosed on the upper surface by the solid-liquid interface. Sn solute redistribution occurs between the equiaxed grains and liquid in the gap. For the same reason, these liquids with enriched Sn solute will flow downward due to gravity. Figure 7b is the microstructure on the lower surface of the HCUS Cu-5wt.%Sn alloy. The equiaxed grains also appear on the lower surface. Sn solute redistribution also occurs between the equiaxed grains and liquid in the gap. Therefore, the lower surface has more Sn content.

In summary, Sn solute will be precipitated from solid to liquid in front of the solid-liquid interface during the HCUS process of Cu-5wt.%Sn alloy. These liquids with enriched Sn solute are pushed to the gap between alloy and mold by the solid-liquid interface. On the upper surface, the liquids with enriched Sn solute flow to the center or lower edge of the alloy due to gravity. Therefore, there hardly exists exudation. On the lower surface, not only Sn solute will be precipitated from solid to liquid, but also, there exist liquids with enriched Sn solute coming from the other part of the alloy due to gravity. These liquids in the gap with a low melting point solidify at the last stage to form an exudation layer of HCUS Cu-5wt.%Sn alloy.

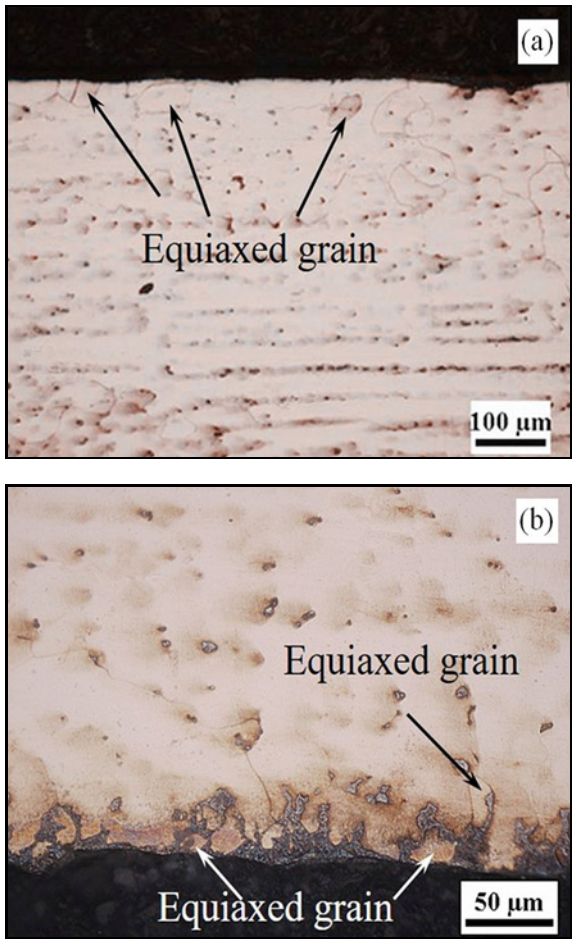


Fig. 7. Microstructure of HCUS Cu-5wt.%Sn alloy: (a) upper surface and (b) lower surface.

## 4. Conclusions

The Cu-5wt.%Sn alloy was prepared by HCUS technology. Meanwhile, the process of HCUS Cu--5wt.%Sn alloy was numerically simulated by Pro--CAST software. The following conclusions are obtained:

(1) There exists exudation layer on the surface of the HCUS Cu-5wt.%Sn alloy. The lower surface has relatively thick exudation, while there is almost no exudation layer on the upper surface of the alloy.

(2) The solute Sn is precipitated to the liquid during the HCUS, resulting in the liquids between den-

drites enrichment of Sn solute. Due to gravity, these liquids pass through the dendrites and flow into the gap between the lower surface and the mold to solidify at last. Thus, an exudation layer rich in low melting point Sn solute on the lower surface is formed.

## References


[1] A. Ohno, Continuous casting of single crystal ingots by the O.C.C. process, JOM 38 (1986) 14–16. https://doi.org/10.1007/BF03257948

[2] F. Yang, J. Wang, J. Yu, Z. Zhou, B. Wang, T. Tu, X. Ren, K. Deng, Z. Ren, Microstructure and mechanical properties of Ni-based superalloy K418 produced by the continuous unidirectional solidification process, J. Mater. Eng. Perform. 28 (2019) 6483–6491. https://doi.org/10.1007/s11665-019-04385-5

[3] Z. Lei, N. Lu, X. Yu, Epitaxy and new stray grain formation mechanism during epitaxial laser melting deposition of Inconel 718 on directionally solidified nickel-based superalloys, J. Manuf. Process. 42 (2019) 11–19. https://doi.org/10.1016/j.jmapro.2019.04.016

[4] S. Kim, W. F. Flanagan, B. D. Lichter, R. N. Grugel, Electrical conductivity in directionally solidified lead-9 and -20 wt pct copper alloys, Metall. Tran. A 24 (1993) 975–979. https://doi.org/10.1007/BF02656519

[5] G. Nie, H. Ding, R. Chen, J. Guo, H. Fu, Microstructural control and mechanical properties of Ti-47Al--2Cr-2Nb alloy by directional solidification electromagnetic cold crucible technique, Mater. Design 39 (2012) 350–357. https://doi.org/10.1016/j.matdes.2012.02.057

[6] I. L. Ferreira, C. A. Siqueira, C. A. Santos, A. Garcia, Theoretical and experimental analysis of inverse segregation during unidirectional solidification of an Al--6.2wt.%Cu alloy, Scripta Mater. 49 (2003) 339–344. https://doi.org/10.1016/S1359-6462(03)00242-2

[7] I. L. Ferreira, C. A. Santos, A. Garcia, V. R. Voller, Analytical, numerical, and experimental analysis of inverse macrosegregation during upward unidirectional solidification of Al-Cu alloys, Metall. Mater. Trans. B 35 (2004) 285–297. https://doi.org/10.1007/s11663-004-0030-8

[8] E. Haug, A. Mo, H. J. Thevik, Macrosegregation near a cast surface caused by exudation and solidification shrinkage, Int. J. Heat Mass Tran. 38 (1995) 1553–1563. https://doi.org/10.1016/0017-9310(94)00286-5

[9] N. Bayat, T. Carlberg, Surface structure formation in direct chill (DC) casting of Al alloys, JOM 66 (2014) 700–710. https://doi.org/10.1007/s11837-014-0950-y

[10] P. Ashtari, K. Gatenby, Formation of inverse segregation on the surface of belt-cast Al-Fe-Si and Al--Fe-Si-Mn alloys, Scripta Mater. 57 (2007) 627–630. https://doi.org/10.1016/j.scriptamat.2007.06.004

[11] S. D. Felicelli, J. C. Heinrich, D. R. Poirier, Simulation of freckles during vertical solidification of binary alloys, Metall. Mater. Trans. B 22 (1991) 847–857. https://doi.org/10.1007/BF02651162

[12] M. C. Flemings, Our understanding of macrosegregation: Past and present, ISIJ Int. 40 (2000) 833–841. https://doi.org/10.2355/isijinternational.40.833

[13] J. H. Luo, Formation Mechanism of Surface Segregation in Heated Mold Continuous Casting Al–Cu Alloy. In: Martin, O. (ed.) Light Metals 2018. TMS 2018. The Minerals, Metals & Materials Series. Springer, Cham. https://doi.org/10.1007/978-3-319-72284-9_59

[14] Y. Xia, F. Wang, J. Wang, G. Li, Simulation of the continuous casting process in a mold of free--cutting steel 38MnVS based on a MiLE method, Int. J. Miner. Metall. Mater. 18 (2011) 562–569. https://doi.org/10.1007/s12613-011-0478-x

[15] J. D. Hwang, H. J. Lin, W. S. Hwang, C. T. Hu, Numerical simulation of metal flow and heat transfer during twin roll strip casting, ISIJ Int. 35 (1995) 170–177. https://doi.org/10.2355/isijinternational.35.170